A Composite 2HDM

S. De Curtis,[1] L. Delle Rose,[2] S. Moretti,[3,4,*] and K. Yagyu[5]

[1]*INFN, Sezione di Firenze, and Department of Physics & Astronomy, University of Florence, Via G. Sansone 1, 50019 Sesto Fiorentino, Italy*

[2]*INFN, Gruppo Collegato di Cosenza, and Department of Physics, University of Calabria, Arcavacata di Rende, I-87036, Cosenza, Italy*

[3]*School of Physics & Astronomy, University of Southampton, Highfield, Southampton SO17 1BJ, United Kingdom*

[4]*Department of Physics & Astronomy, Uppsala University, Box 516, 75120 Uppsala, Sweden*

[5]*Department of Physics, Osaka University, Toyonaka, Osaka 560-0043, Japan*

*(*Speaker)*

Abstract

We review the collider phenomenology of a 2-Higgs Doublet Model (2HDM) arising within (partial) Compositeness, wherein all Higgs states are pseudo Nambu-Goldstone Bosons (pNGBs) emerging from a $\mathrm{SO}(6) \to \mathrm{SO}(4) \times \mathrm{SO}(2)$ breaking in a new strong sector and their properties are obtained in terms of the fundamental parameters of the Composite sector, such as masses, Yukawa and gauge couplings of new spin-1/2 and spin-1 resonances.

Keywords: Extended Higgs Sectors, Compositeness, Colliders
DOI: 10.31526/ACP.BSM-2023.14

1. INTRODUCTION

Compositeness appears as a viable theory of the Electro-Weak (EW) scale as it can naturally solve the hierarchy problem of the Standard Model (SM): any energy at which the Higgs boson mass is probed is naturally converted into motion of the constituents, up to an energy scale, characterising the dynamics of a new strong sector, beyond which the Higgs state may start breaking apart. Such an idea is modelled upon Quantum Chromo-Dynamics (QCD): the SM Higgs state, emerging as a pseudo-Nambu-Goldstone Boson (pNGB) following a $G \to H$ spontaneous breaking and the explicit one of H via (gauge) and (Yukawa) mixings to generate an effective (i.e., at loop level) scalar potential, in turn triggering EW Symmetry Breaking (EWSB) using the Higgs mechanism, is the lowest lying Composite object.

Hence, such a Higgs state, discovered in 2012 at the Large Hadron Collider (LHC), could be the analogue of the pion of the standard QCD interactions. Furthermore, just like there are additional mesons predicted by QCD, π, η, etc., there could also be several new Higgs states predicted by Compositeness beyond the one discovered so far (henceforth, denoted by h), as well as additional Composite states with different spin (the equivalent of the ρ, ω, etc. of QCD). In this respect, a natural setting (as initially emphasised in [1]) is the Composite 2-Higgs Doublet Model (C2HDM), eventually explicitly realised in Refs. [2, 3, 4]. Such a construct is built by enlarging the coset associated to the breaking of the global symmetry of the underlaying strong interactions to contain, besides the SM-like Higgs doublet, an additional one. The presence of an extra Higgs doublet is not unusual in model building, e.g., it is naturally expected in Supersymmetry (SUSY), another viable theory of the EW scale, in the form of the Minimal Supersymmetryc Standard Model (MSSM). A comparative study between the 2HDM arising from Composite dynamics and the one realised in SUSY models has been presented in [5].

Here, we focus on the Higgs sector of the C2HDM originating from the breaking $\mathrm{SO}(6) \to \mathrm{SO}(4) \times \mathrm{SO}(2)$ in presence of *partial Compositeness* [6] involving the third generation of SM fermions. The masses of all Higgs bosons of the C2HDM and their self-interactions are generated starting at one-loop level via the Coleman-Weinberg (CW) potential by the linear mixing between the (elementary) SM and the (Composite) strong sector fields. As such, the Higgs masses and couplings are not free parameters, unlike in (non-SUSY) realisations of the 2HDM with fundamental Higgs bosons, but depend upon the strong sector dynamics and present strong correlations among themselves, which is one of the main features of Composite Higgs Models (CHMs) in general. Also, notice that the aforementioned scalar potential can effectively be constructed under the usual conditions of vacuum stability, perturbativity, unitarity, etc. and can produce phenomenolgical manifestations [7, 8, 9] notably different from those of Elementary 2HDMs (E2HDMs) [10].

The scale of Compositeness f is typically within the energy reach of the LHC and the Composite nature of the SM-like Higgs boson in the C2HDM can be accessed by exploiting the corrections of $\mathcal{O}(\xi)$ to its couplings, where $\xi = v_{\mathrm{SM}}^2/f^2$ with v_{SM} being the Vacuum Expectation Value (VEV) of the Higgs state in the SM. Since current (lower) limits on f are of order 700–800 GeV, such deviations affect experimental observables only at the 5–10% level making their observations a quite difficult task for the LHC. For example, the $\mathcal{O}(\xi)$ corrections in the Yukawa interactions with top- and bottom-(anti)quarks or tau-(anti)leptons are notoriously difficult to measure at the LHC as they are affected by significant QCD background. A much cleaner alternative is to probe the interactions of the SM-like Higgs state with the gauge bosons, which are also affected by similar $\mathcal{O}(\xi)$ corrections.

Such a corrections are accessible at, possibly, the LHC during Run 3 and at, certainly, the High Luminosity LHC (HL-LHC) [11], with 1000 fb^{-1} of annual luminosity, and/or the High-Energy LHC (HE-LHC), with 27 TeV as Centre-of-Mass (CM) energy.

However, even if C2HDM predictions were to be found consistent with the E2HDM ones, one could still disentangle the Composite and fundamental realisations of a 2HDM by exploiting the correlations among several observables of the various Higgs bosons. Hence, under the above circumstances, it becomes mandatory to explore the scope of the aforementioned HL-LHC and HE-LHC, as differences are more manifest in processes involving Higgs boson self-couplings, which have rather small cross sections at the current LHC (so we will specifically be discussing di-Higgs production at all such collider setups, which indeed involves trilinear Higgs self-couplings).

In the following, after briefly sketching the C2HDM and defining its parameter space, we study, first, differences between the C2HDM and the aforementioned MSSM. Then, we illustrate how the C2HDM may reveal itself via virtual effects of top-(anti)quark spin-1/2 companions[1] in SM-like Higgs pair production in the continuum via $gg \to hh$ in non-resonant searches as well as via real particle effects due to a heavy CP-even Higgs state entering the same process in resonant searches. Finally, we report on under which CERN machine configurations one can access the resonant processes $gg \to H \to hh \to b\bar{b}\gamma\gamma$ and $gg \to H \to t\bar{t}$ (in the semi-leptonic decay channel), which can be exploited to extract crucial features of the C2HDM, where H and h are the heaviest and the lightest (the SM-like one) of the two CP-even neutral Higgs states, respectively. (For a review of C2HDM phenomenological manifestation at future e^+e^- colliders, see Ref. [12].) This mini-review is based on Refs. [3, 4, 5], from where all figures and some of the textual material are taken.

2. PHENOMENOLOGY

Here, we provide some sample results charactering the phenomenology of the C2HDM.

2.1. Model Construction and Parameter Space Definition

The structure of the model is described in detail in Refs. [4, 5], to which we refer the reader. The fundamental parameters of the C2HDM are as follows: the Compositeness scale f, the gauge coupling of the new strong interaction g_ρ, the masses and Yukawas of the heavy top partners as well as the mixing between the latter and the elementary top quark (which represents the leading contribution to the CW effective potential), see Section 4.1.1 of [4]. The corresponding parameter space has been explored by scanning the Compositeness scale over the interval $(750, 3000)$ GeV and all other mass dimension inputs over the $(-10, 10)f$ range[2]. We select phenomenologically viable parameter configurations by requiring: (i) the vanishing of the two tadpoles of the CP-even Higgs bosons, (ii) the predicted top mass to be 165 GeV $< m_t <$ 175 GeV and (iii) the predicted SM-like Higgs boson mass to be 120 GeV $< m_h <$ 130 GeV. (The more relaxed tolerance on the two latter observables than the actual error on their experimental measurements is due to the fact that we compute these parameters at lowest order.) The masses of the heavier CP-even Higgs boson (m_H), the charged Higgs boson ($m_{H^\pm}$), the CP-odd Higgs boson (m_A), the mixing angle θ between the two CP-even states (h, H) and their couplings to fermions and bosons are all obtained from the fundamental parameters of the new strong sector.

These quantities are then tested against experimental measurements through the HiggsBounds [13] and HiggsSignals [14] packages, providing, respectively, constraints from null extra Higgs boson searches and measurements of the discovered Higgs state. (We have re-tested the parameter space of the C2HDM against HiggsTools [15] and found no significant differences from the results presented here.) The derived C2HDM couplings, expressed in the κ 'coupling modifier' scheme [16], are used as extracted after Run 1 and Run 2 as well as extrapolated to 300 fb^{-1} (end of Run 3) and 3000(15000) fb^{-1} at the HL-LHC(HE-LHC) by adopting the expected experimental accuracies given in scenario 2 of Ref. [17]. Among such κ modifiers, those interesting in our case are especially κ^h_{VV} ($V = W, Z$), $\kappa^h_{\gamma\gamma}$ and κ^h_{gg}, which are, typically, the most constraining ones.

Just like in the E2HDM case, a completely general C2HDM Lagrangian introduces Higgs-mediated Flavour Changing Neutral Currents (FCNCs) at tree level via Higgs boson exchanges. In order to control these, we adopt an alignment (in flavour space) configuration between the Yukawa matrices as done in the (elementary) Aligned 2HDM (A2HDM) [18]. In this scenario, the coupling of the heavy Higgs H to the top quark is controlled (plus some small corrections induced by the mixing angle $\theta \sim v^2/f^2$) by

$$\zeta_t = \frac{\bar{\zeta}_t - \tan\beta}{1 + \bar{\zeta}_t \tan\beta}, \tag{1}$$

where $\bar{\zeta}_t$ (defined in [4]) and $\tan\beta$ (given, as usual, by the ratio of the two Higgs field VEVs) are predicted and correlated to each other, in terms of the fundamental parameters of the C2HDM strong sector. Being, in particular, interested in the phenomenology of the heavy Higgs states, we map the results of our scan in terms of, e.g., m_H and ζ_t and we restrict the parameter space to the region $m_{H,A,H^\pm} > 2m_h$. As an example of the correlations between observables mentioned above, we show in Figure 1 the mass splitting between the CP-odd state,the heavy CP-even one and the charged Higgs ones.

Even though we assume a flavour symmetric Composite sector, there are modifications to rare flavour transitions in the SM induced by the exchange of the pNGBs. The bound from the $B \to X_s\gamma$ process depends on the interplay between the top and the bottom contributions and, in particular, on the relative size of the charged Higgs $H^\pm$ couplings to the top and bottom quarks, ζ_t and ζ_b, respectively. In the scenario discussed in Ref. [4], in which $\zeta_t = \zeta_b$, the excluded region from $B \to X_s\gamma$ is shown in Figure 2, by the red shading. In different scenarios providing $\zeta_b < \zeta_t$, the bound can be relaxed such that all points can survive the constraint. In

[1] In doing so, we will instead decouple the new spin-1 states.

[2] We note that all scan points are randomly generated, so that their density is a measure of probability of a region of parameter space to meet any constraints imposed.

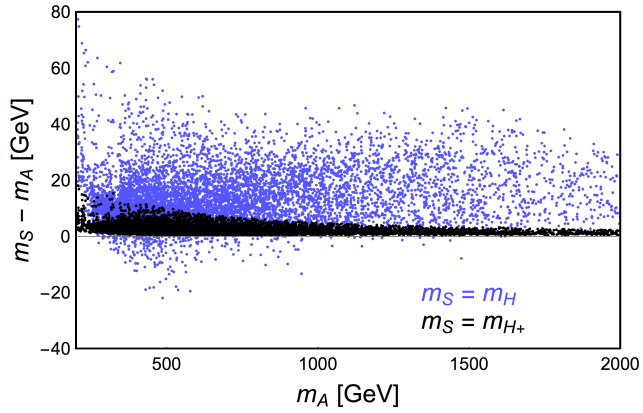

FIGURE 1: Mass splittings $m_H - m_A$ (blue) and $m_{H^+} - m_A$ (black) versus m_A.

contrast, the bound from the $B_s \to \mu^+\mu^-$ transition is more robust as it only depends on ζ_t. However, the corresponding excluded region does not overlap with the distribution of acceptable points.

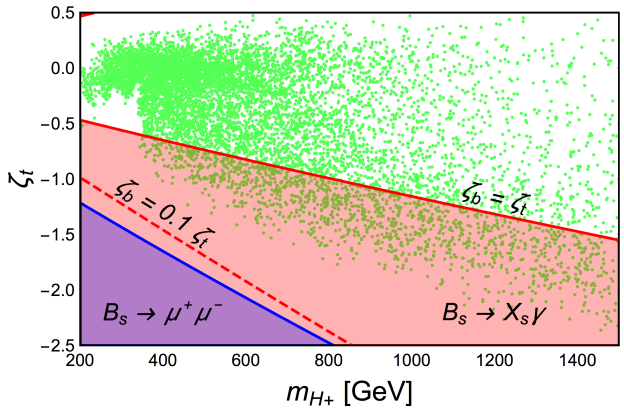

FIGURE 2: Correlation between the charged Higgs mass m_{H^+} and the corresponding coupling to the top quark. Green points are allowed by current LHC direct and indirect searches. Red and purple regions are excluded at 2σ level by measurements of the $B \to X_s\gamma$ (under the assumption $\zeta_b = \zeta_t$) and of $B_s \to \mu^+\mu^-$ transitions, respectively. The former bound strongly depends on the size of ζ_b.

2.2. *C2HDM versus MSSM*

We highlight next the main differences between the C2HDM and MSSM, both of which can be regarded as the minimal realisations of EWSB based on a 2HDM structure embedded in the fundamental theories of Compositeness and SUSY, respectively. (Notice that, in the MSSM, the Yukawa structure is a Type-II one). In order to study the phenomenology of the MSSM, we use the code `FeynHiggs 2.14.1` [19, 20] and scan its parameter space by adopting the recommendations of [21].

2.2.1. *Prediction of* $\tan\beta$ *and Higgs Boson Masses*

While, in the MSSM, $\tan\beta$ is is a free parameter, which can be limited by theoretical and experimental conditions, in the C2HDM, it is a predicted quantity and is correlated rather strongly to f. This is well exemplified in Figure 3. Herein, the density of the allowed points become smaller in regions with larger values of f and/or $\tan\beta$. This can be understood in terms of the following: any departure from $f \sim v_{\rm SM}$ requires fine-tuning amongst the parameters in the new strong sector: indeed, this is in order to satisfy the tadpole conditions and reproduce the observed m_h and m_t values, as aslready noted in more minimal versions of CHMs [22]. Therefore, in the C2HDM, while configurations with small f (i.e., within the LHC energy reach) and $\tan\beta \sim \mathcal{O}(1)$ are naturally predicted, solutions with $\tan\beta \sim 10$ or larger are highly disfavoured by imposing $m_h \sim 125$ GeV and $m_t \sim 170$ GeV, no matter the value of f. In addition, for any f value, we notice that $\tan\beta$ values between about 1 and 6 are more favoured than others: thus, in the following, we will at times concentrate on this specific region of C2HDM parameter space.

However, this result on $\tan\beta$ does not imply that the parameter space of the Higgs sector of the C2HDM is smaller with respect to the MSSM one. While it is true that in the latter scenario such a parameter can in general take values between 1 and, say, $\bar{m}_t/\bar{m}_b \approx 45$, where $\bar{m}_{b,t}$ are the running masses of the b,t-(anti)quarks (evaluated at m_h), compatibly with SUSY unification

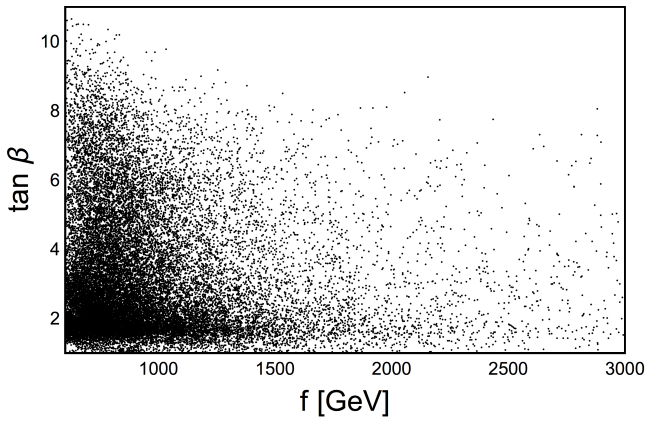

FIGURE 3: Prediction of f and $\tan\beta$ in the C2HDM.

conditions as well as theoretical and experimental constraints, it should also be recalled that $\tan\beta$ is not, in general, a fundamental parameter of a 2HDM, as discussed in Refs. [23, 24, 25], since it is not basis-independent. Therefore, any one-to-one comparison of models for fixed values of $\tan\beta$ is not meaningful unless the realisation of the 2HDM is the same, namely, the models share the same discrete symmetries. While the MSSM is characterised by a Type-II 2HDM structure, with $\tan\beta$ defined in the basis where the discrete symmetry of the two Higgs doublets is manifest, the C2HDM considered in this work does not possess a Z_2 (or, rather, a C_2) symmetry. Even though the strong sector uniquely identifies a special basis for the Higgs states and, thus, selects a special $\tan\beta$ among all possible basis-dependent definitions (see [4] for more details), this parameter cannot be directly compared to the MSSM one. Therefore, when comparing the physical observables in the two scenarios that we have picked (Compositeness and SUSY), one should inclusively span $\tan\beta$ between 1 and 45 for the MSSM and over all predicted values (see Figure 3) for the C2HDM, which is what we shall do in hereafter.

Other than $\tan\beta$, also the masses of all Higgs states are predicted in the C2HDM, as discussed already. While we have previously remarked that some level of degeneracy exist amongst m_H, m_A and $m_{H^\pm}$ (recall Figure 1), here, we want to discuss their dependence upon f, which is done for, e.g., m_A, in Figure 4. We find that larger values of m_A are obtained for larger f and/or $\tan\beta$. The reason for such a dependence is that the mass of the CP-odd state is not directly constrained by the tadpole conditions and it is naturally of order f. In particular, one can show that $m_A^2 \simeq c(1+\tan^2\beta)f^2$, where $c \approx 0.05$ may vary by a factor of 2 only for $\tan\beta \lesssim 1$. All these features remain stable against different choices of $g_\rho > 1$. The pattern for $m_{H^\pm}$ is not very different while, for m_H, a combination of the tadpole conditions and the θ dependence of the elements of the CP-even mass matrix contribute to a more noticeable spread of points (for fixed $\tan\beta$), in turn responsible for what seen in Figure 1 (see also Figure 6 below).

2.2.2. Alignment with Delayed Decoupling

Beside the Higgs mass spectrum, additional physics observables that can be used to tension the C2HDM against the MSSM are, e.g., Higgs cross sections (σ) and Branching Ratios (BRs). A straighforward fashion to compare the two is to recast Higgs sector parameters in the language of the aforementioned κ modifier. In this framework, we look here at κ_V ($V = W, Z$), this being the most precisely known of all κ's. In the C2HDM, one has

$$\kappa_V = \left(1 - \frac{\xi}{2}\right)\cos\theta, \quad \xi \equiv \frac{v_{\rm SM}^2}{f^2}, \tag{2}$$

where $\theta \to 0$ with $f \to \infty$ corresponds to the alignment limit, i.e., the couplings of h to SM particles become the same as those of the SM Higgs boson (at tree level). Figure 5 shows that the (near) alignment limit ($\kappa_V \sim 1$) is reached at large Higgs boson masses (again, exemplified here by the CP-odd one) in both the C2HDM and MSSM. Yet, in the MSSM, κ_V very quickly reaches 1. In contrast, in the C2HDM, it reaches 1 slowly (and how slowly this happens depends on $\tan\beta$). This delayed decoupling is driven by the negative $\mathcal{O}(\xi)$ corrections which are typical of CHMs, as seen in Eq. (2), combined with the fact that the slopes seen in Figure 5 for the C2HDM exhibit the dependence of m_A upon f illustrated in Figure 4, which allows a different and wider spread of κ_V values away from 1 with respect to the MSSM. In practice, the typical dependence of the MSSM points is $1-\kappa_V \sim v^4/m_A^4$ while in the C2HDM one has $1-\kappa_V \sim \xi/2 \sim v^2/m_A^2$. We note that values of $\kappa_V \gtrsim 0.9$ are currently compatible with LHC data at 1σ level [26], therefore, if a large deviation in the hVV coupling from the SM prediction will be established by future experiments, it will imply a larger Compositeness scale in the C2HDM. Conversely, if such a deviation will instead be established and no heavy Higgs state below 400 GeV or so will be seen, the MSSM may be ruled out and the C2HDM could instead explain the data. Therefore, either way, by combining the measured value of κ_V to that of an extracted or excluded m_A, one may be able to discriminate between the MSSM and C2HDM.

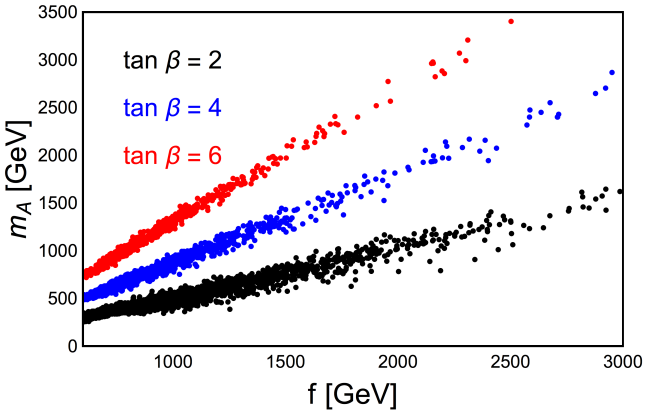

FIGURE 4: Prediction of m_A as a function of f in the C2HDM for $\tan\beta = 2$, 4 and 6.

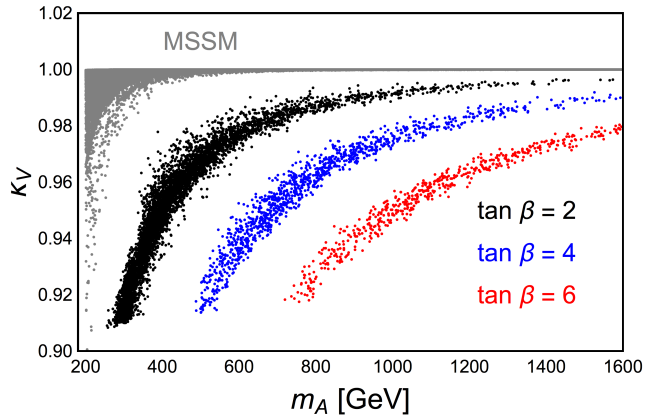

FIGURE 5: Comparison in the correlation of m_A versus κ_V between the C2HDM and MSSM for $\tan\beta = 2, 4$ and 6 in the former and all values of $\tan\beta$ in the latter.

2.2.3. Mass Hierarchy Amongst Heavy Higgs States

Figure 6 shows the mass differences $m_{H^\pm} - m_A$ and $m_H - m_A$ where $\tan\beta$ has been varied over all its possible values in our two reference models, as explained above. We find that (top frame), while $m_{H^\pm}$ and m_A are very close in the C2HDM, within 5 GeV, larger mass differences between these two heavy Higgs bosons are allowed in the MSSM, particularly for smaller m_A, e.g., $m_{H^\pm} - m_A$ can reach $\approx$ 30 GeV for $m_A = 200$ GeV[3]. Due to the particular structure of the scalar potential, the contribution of the fermionic sector cancels out in the mass splitting of A and $H^\pm$ and only the gauge sector one survives. The latter can be approximated by $(m_{H^\pm} - m_A)/m_A \simeq g'^2\xi$, with g' the hypercharge gauge coupling. This represents a robust prediction of the model. Conversely, for $m_H - m_A$ (bottom frame), it is the other way around. With increasing m_A, starting from 300 GeV, the mass difference between the two heavy neutral Higgs bosons tends to be confined within 5 GeV or so for the MSSM while in the C2HDM this can range from -40 GeV (at moderate m_A) to $+40$ GeV (for larger m_A). The mass splitting is not strictly determined as in the $m_{H^\pm} - m_A$ case but can be, nevertheless, estimated by $(m_H - m_A)/m_A \simeq c'\,\xi$ with c' being an order 0.1 coefficient encoding the dependence on the fermionic parameters of the strong sector. The ξ factor, appearing in the formulae of the mass splittings, reproduces the expected mass degeneracy among A, H and $H^\pm$ in the large f regime. Interestingly then, the hierarchy amongst $m_{H^\pm}$, m_A and m_H may enable one to distinguish between the two scenarios as (recalling that three-body decays via off-shell gauge bosons are possible) establishing $H^\pm \to W^{\pm *}A$ would point to the MSSM while extracting $H \to Z^*A$ or $A \to Z^*H$ would favour the C2HDM.

2.3. Di-Higgs Production

Here, we investigate the spectrum of the top-(anti)quark companions in the C2HDM, eight of these, denoted as T_i ($i = 1, ...8$). Needless to say, just like the Higgs masses, the Composite top-(anti)quark partner masses are strongly correlated to f. In Figure 7, we show, e.g., the correlation between f and the lightest top partner mass M_{T_1}. Here, we can see that the $\tan\beta$ dependence is rather unimportant. In particular, we find that typically a minimum M_{T_1} is obtained and such a lower limit gets higher as f increases. For a given f, the minimum allowed value of M_{T_1} is $\sim f$ and it is strictly determined by the reconstruction of the top mass from the parameters of the strong sector. This behaviour agrees with well-established results in minimal CHMs [22]. A distinctive feature

[3]Recall that, In the MSSM, m_A is normally taken, together with $\tan\beta$, as an input value to uniquely define the Higgs sector at tree level.

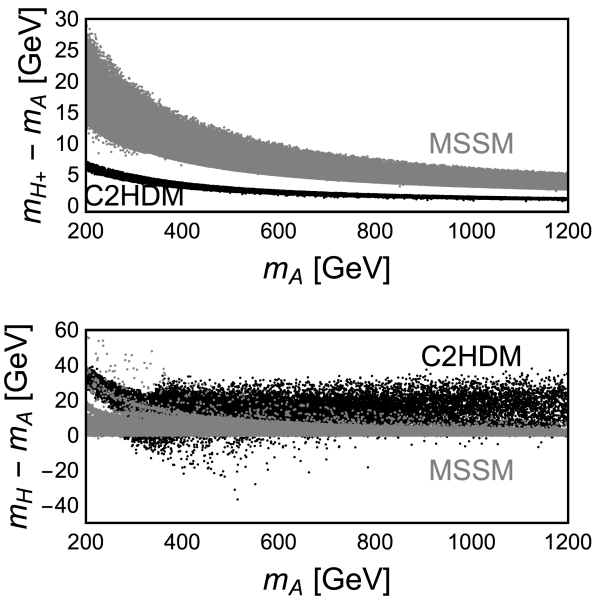

FIGURE 6: Comparison in the correlation of m_A versus $m_{H^\pm} - m_A$ (top) and $m_H - m_A$ (bottom) between the C2HDM and MSSM for all values of $\tan\beta$ in both scenarios.

between the C2HDM in connection with the heavy top sector is the fact that the measured value of $m_h \sim 125$ GeV requires a fermionic top-(anti)quark partner in the C2HDM which is sub-TeV. The lightest 2/3 fermion partner in the C2HDM (T_1) is then potentially accessible at the LHC whatever the actual m_h value, see Figure 8. However, rather than studying the production of T_i states as real objects in the final state, here, we concern ourselves with their virtual effects in SM processes. Specifically, we look at the process $gg \to hh$ at the LHC, given by the Feynman diagrams in Figure 9.

2.3.1. Non-Resonant Di-Higgs Production

We start by looking at when the cross section of the above process is not dominated by resonant production. As detailed in Ref. [27], we include in this definition scenarios where the contribution of the s-channel topology $gg \to h, H \to hh$ is $< 10\%$ of the total cross section, i.e., after applying the condition given in Eq. (5.20) of Ref. [27]. We will first discuss the inclusive results and then move on to differential distributions, by investigating the effect of the different diagrams and the resulting interferences.

Inclusive Results In Figure 10 we display, as a function of f, the Leading Order (LO) cross section of the above process in the C2HDM normalised to the SM value for the non-resonant points, which we obtained from our sample of allowed configurations. For small f, non-resonant production in the C2HDM can be up to a factor of ≈ 2.3 times larger than SM value. However, it can also be smaller by up to a factor of ≈ 0.5 the SM value. The current limit from a recent ATLAS study combining several final states lies at 2.4 the SM value at 95% Confidence Level (CL) [28], so that the C2HDM could soon be tested at Run 3 of the LHC in non-resonant searches.

Exclusive Results For the discussion of the exclusive results, we selected Benchmark Points (BPs) displaying some interesting features, all summarised in [27]. In Figure 11 we show the invariant mass ($Q \equiv m_{hh}$) distribution for a BP with a heavy Higgs boson mass of 2.98 TeV. The distribution shows a local enhancement at that Q value, but the corresponding cross section contribution is indeed negligible. Let us then note that, for this BP, neglecting the heavy quarks, i.e., only taking into account diagrams with a top quark in the loop (orange line), results in a distribution that is below the SM expectation (blue line), until about 1.6 TeV. Furthermore, the distribution obtained by additionally neglecting the quartic 2-Higgs-2-fermion coupling (red), entering the diagram on the right of Figure 9, is always above the SM expectation. We can therefore clearly see for this BP a destructive interference involving the quartic coupling. If we look then at the distribution for the full cross section including all diagrams (light blue), we are back at around the SM expectation (so, the constructive interference of the heavy quarks and the destructive one due to the quartic coupling cancel each other), at least below the onset of the heavy quark effects at the threshold of $2m_{T_8} \approx 2.6$ TeV. This last feature, if detected, would clearly indicate the presence of new physics in di-Higgs production.

2.3.2. Resonant Di-Higgs Production

We now turn to the discussion of the resonant case both inclusively and exclusively. That is, here, we discuss a BP that exhibits a clear resonant peak in the distributions, thus contributing substantially to the total cross section.

Inclusive Results In Figure 12, red points fullfill all constraints while blue points are excluded by resonant di-Higgs searches at the LHC (see [27]). Again, we show the inclusive cross section normalised to the SM value but now as a function of m_H (rather than f). Here, we see that we can have a significant enhancement of the cross section, by up to more than 30 times the SM one. Such large rates are, however, excluded (blue points). Hence current resonant searches are already sensitive to the explored parameter region.

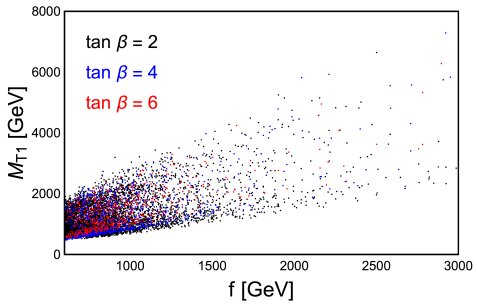

FIGURE 7: Correlation of M_{T_1} versus f in the C2HDM for $\tan\beta = 2$, 4 and 6.

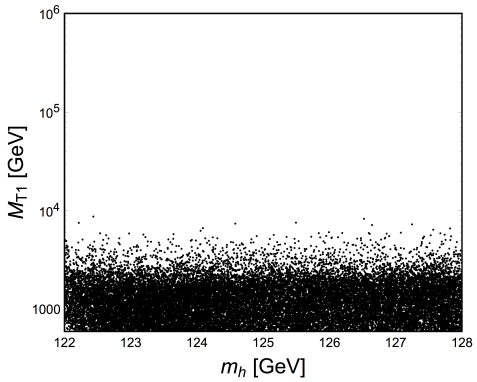

FIGURE 8: Correlation of m_h versus M_{T_1}, the mass of the lightest 2/3 fermionic partner in the C2HDM, for all values of $\tan\beta$.

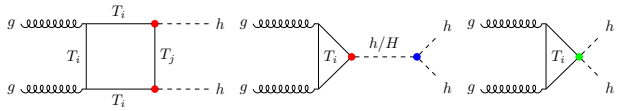

FIGURE 9: Generic diagrams contributing to SM-like hh production via gg fusion in the C2HDM, mediated by the SM top (denoted by T_9) and the heavy top partner (denoted by $T_1, ..., T_8$) loops ($i, j = 1, ..., 9$). The coloured dots indicate the new (green) and modified (red and blue) interactions relative to the SM.

The maximal cross section allowed by experiment in our sample is around 10 times the SM value. Furthermore, as can be inferred from the plot, with increasing m_H (which corresponds to increasing f, as previously discussed) one obtains the SM result.
Exclusive Results In Figure 13 we can see a BP with a clear resonance at the heavy Higgs mass $m_H = 1.2$ TeV and also a visible threshold effect for the lightest heavy top partner T_8 at $Q \approx 2.7$ TeV. Due to the relatively large Higgs mass, the effect of the resonance contribution on the total cross section is rather small so that we obtain a cross section value of the order of the SM expectation. The shape of the differential cross section, however, is quite interesting since we have several contributions, stemming from the heavy resonance, the heavy top partners and the quartic 2-Higgs-2-fermion coupling, which can all interfere with each other. In the plot, the E2HDM-like limit is given by the red curve, when the heavy quarks and the quartic 2-Higgs-2-fermion couplings are both turned off. We then see that, in this example, the full cross section (light blue line) is enhanced compared to the SM value (blue line) both before and after the resonant peak, thus, in contrast to the E2HDM-like result. In the latter case there is only the triangle diagram with the heavy Higgs which interferes with the SM-like triangle and box diagrams. The interference term is proportional to $(Q^2 - m_H^2)$ and hence changes sign at the resonance mass. When we additionally add in the contribution of the diagram with the quartic 2-Higgs-2-fermion coupling (orange line), which in this example interferes in such a way that we have a suppression before the resonance and an enhancement after the resonance. Adding in also the heavy quarks, we have the complete model (light blue line) and their contribution finally leads to the described behaviour of the distribution. Thus, in principle, the interference patterns around a resonance can be used to distinguish between an E2HDM and the C2HDM.

2.3.3. Future Colliders

Here, we look at possible decay channels of hh pairs and establish the sensitivity of the current LHC (after Run 3) as well as future configurations of it, such as the aforementioned HL-LHC and HE-LHC. For reasons of space, we limit ourselves to the case of resonant production, i.e., the process $gg \to H \to hh$.

The parameter ζ_t and the trilinear coupling λ_{Hhh} control the hierarchy amongst the decay modes of the heavy H state. In particular, $H \to t\bar{t}$, when kinematically allowed, represents the dominant decay channel. Below the $t\bar{t}$ l threshold at $m_H \approx 2m_t$, the $H \to hh$ mode can reach $\sim 80\%$ while the remaining total width is saturated by $H \to VV$ ($V = W, Z$). The corresponding BRs are

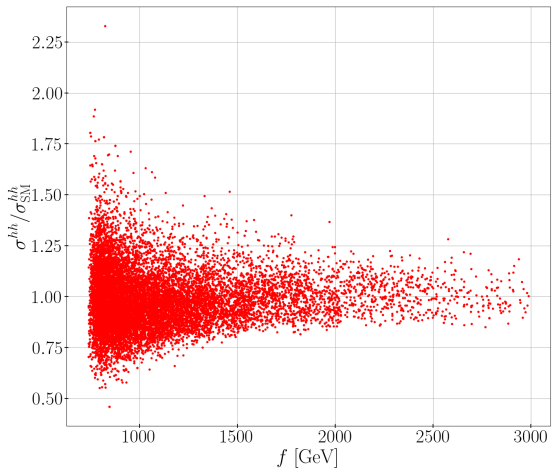

FIGURE 10: The full cross section of non-resonant points normalised to the SM cross section plotted against the compositeness scale f.

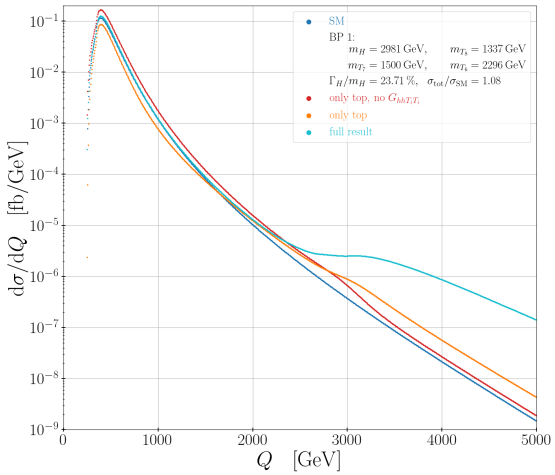

FIGURE 11: Invariant mass distribution for BP1 of [27]. Blue: SM result; light blue: full C2HDM result; orange: C2HDM including only top loops; red: C2HDM with only top loops and no quartic 2-Higgs-2-fermion coupling. We also indicate the heavy Higgs mass and total width to mass ratio and the masses of the three lightest heavy top quarks as well as the ratio of the total inclusive C2HDM cross section to the SM value.

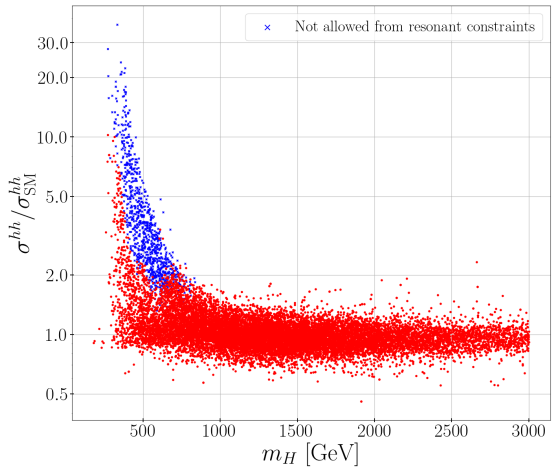

FIGURE 12: The total cross section normalised to the SM result, plotted against m_H, where the blue points are excluded by resonant searches.

shown in the top panel of Figure 15 and these can be much different in the C2HDM with respect to E2HDMs, since the *Hhh* and

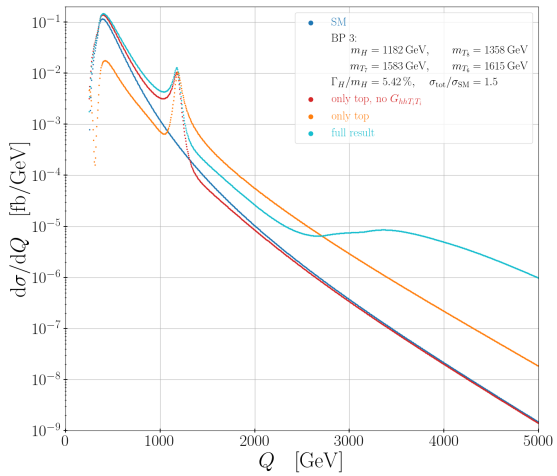

FIGURE 13: Invariant mass distribution for the BP3 of of [27]. Colour codes as in Figure 11.

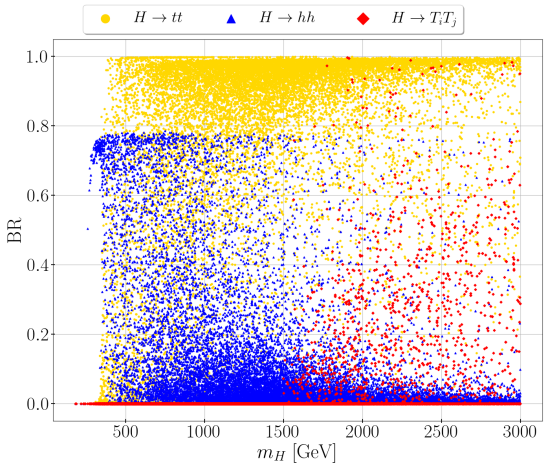

FIGURE 14: The BRs of the C2HDM heavy H boson as a function of its mass in the following decay channels: tt (yellow), hh (blue), and T_iT_j with $i \neq j$ (red) and at least one being a heavy top quark with all possible final states been summed up.

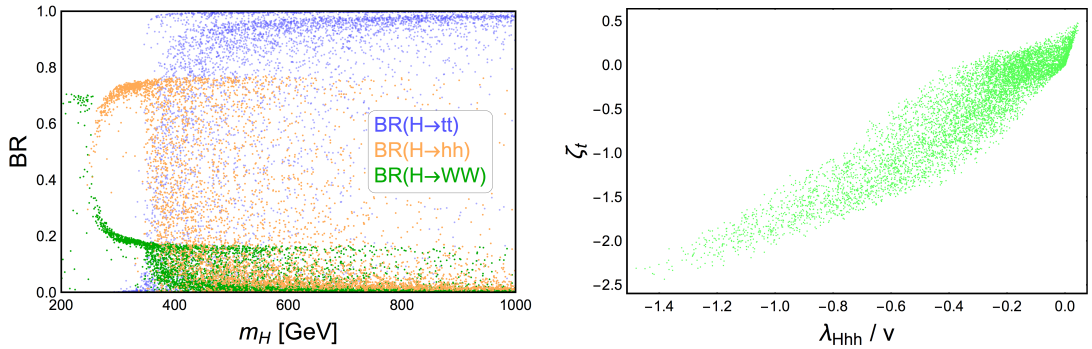

FIGURE 15: (Top) The BR of the H boson of the C2HDM as a function of its mass in the following decay channels: WW (green), hh (orange) and $t\bar{t}$ (blue). (Bottom) the correlation between the couplings ζ_t and λ_{Hhh} obtained upon imposing current HiggsBounds and HiggsSignals constraints at 13 TeV.

$Ht\bar{t}$ interactions carry the imprint of Compositeness (their correlation is shown in the bottom plot of Figure 15). In other words, the relative size of the $H \to hh$ and $H \to t\bar{t}$ decay modes highlights their key role in the discovery and characterisation of the Composite H state.

Figure 16 (top) shows the interplay between direct and indirect searches and the capabilities of the HL-LHC and HE-LHC in discovering the $gg \to H \to hh \to b\bar{b}\gamma\gamma$ signal over regions of the C2HDM parameter space projected onto the plane (m_H, ζ_t), even when no deviations are visible in the κ modifiers of the SM-like Higgs state h (red points) with luminosities $L = 300$ fb^{-1} and $L = 3000$ fb^{-1}. The 95% Confidence Level (CL) exclusion limits have been extracted by employing the sensitivity projections

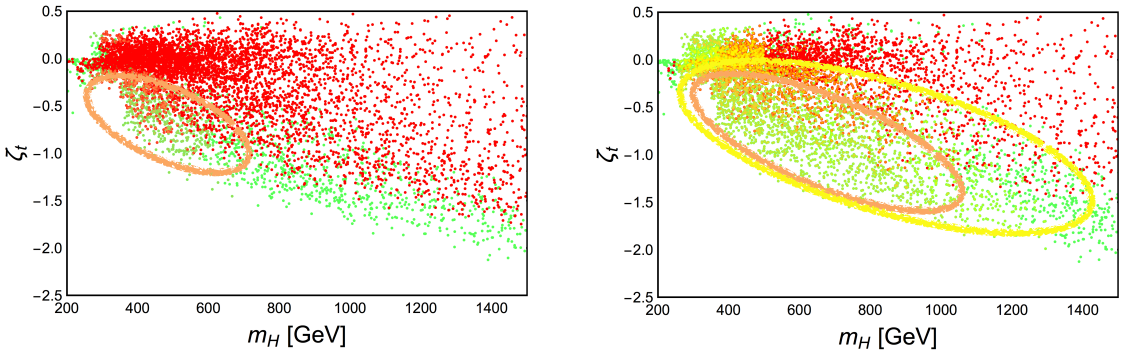

FIGURE 16: Results of the C2HDM scan described in the text. Colour coding is as follows. Green: all points that pass present constraints at 13 TeV. Red: points that, in addition to the above, have κ^h_{VV}, $\kappa^h_{\gamma\gamma}$ and κ^h_{gg} within the 95% CL projected uncertainty at $L = 300$ fb^{-1} (top) and $L = 3000$ fb^{-1} (bottom). Orange: points that, in addition to the above, are 95% CL excluded by the direct search $gg \to H \to hh \to b\bar{b}\gamma\gamma$, at $L = 300$ fb^{-1} (left) and $L = 3000$ fb^{-1} (right). In the right plot the yellow points are 95% CL excluded by the same search at the HE-LHC with $\sqrt{s} = 27$ TeV and $L = 15$ ab^{-1}. The orange and yellow elliptical shapes highlight the regions in which the points of the corresponding colour accumulate.

declared in [29] and [30] while compliance with the coupling modifiers has been achieved by asking that $|1 - k^h_i|$ is less than the uncertainty discussed in Ref. [17], with $i = VV, \gamma\gamma$ and gg. Notice that the orange points have a large overlap with the red ones for small values of $|\zeta_t|$. As shown in [31], $gg \to H \to t\bar{t}$ (followed by semi-leptonic decays) would also allow to probe larger values of m_H. Therefore, the $gg \to H \to hh$ process enables one to cover a larger C2HDM parameter space while the $gg \to H \to t\bar{t}$ one higher H masses. As such, the combination of the two allows to obtain the benefits of either. The HE-LHC, assuming $\sqrt{s} = 27$ TeV and $L = 15$ ab^{-1}, will improve the reach in the H high mass region up to 1.3 TeV by studying the process $gg \to H \to hh \to b\bar{b}\gamma\gamma$ (bottom plot in Figure 16). Concerning the $gg \to H \to t\bar{t}$ channel, the naive extrapolation of the sensitivity with the parton luminosities at the HE-LHC is unreliable because it is affected by the $t\bar{t}$ threshold effects. We also remark that for a proper phenomenological analysis of the $t\bar{t}$ process, the interference effects with gg-induced irreducible background must be fully taken into account [32]. In particular, the interference effects between the gg-induced QCD diagrams at LO and the one providing a Higgs boson in s-channel via gluon fusion generate a peak-dip structure of the $m_{t\bar{t}}$ spectrum that could sensibly affect the sensitivity reach of this process.

3. CONCLUSIONS

In summary, in view of the phenomenological results presented here for the C2HDM, in presence of up-to-date theoretical and experimental constraints, we are confident to have highlighted the main distinctive features between this scenario and customary E2HDMs (including the MSSM), which can be tested at the current LHC by the end of its current stage (Run 3) as well as those already scheduled (HL-LHC) or discussed (HE-LHC). These different manifestations have been illustrated in all components of our Composinetess scenario, i.e., the gauge (albeit neglecting the presence of new Composite gauge bosons), fermion (specifically to the case of new heavy top-(anti)quark states) and (2HDM) Higgs sector. In all such contexts, signals of the C2HDM may emerge at the aforementioned CERN machine configurations, distinctively different from those pertaining to E2HDMs (including the MSSM), above and beyond systematic and statistical errors, so as to motivate dedicated experimental analyses of this intriguing theoretical construct, which represents the Compositeness version of the time-honoured MSSM within Supersymmetry.

ACKNOWLEDGEMENTS

SM is supported in part through the NExT Institute, STFC Consolidated Grant No. ST/L000296/1 and Knut and Alice Wallenberg foundation under the grant KAW 2017.0100 (SHIFT). Some of us are also grateful to Felix Egle, Margarete Mühlleitner and Kodai Sakurai for collaborating on some aspects of the content of this review.

References

[1] J. Mrazek, A. Pomarol, R. Rattazzi, M. Redi, J. Serra and A. Wulzer, Nucl. Phys. B **853** (2011), 1-48 [arXiv:1105.5403 [hep-ph]].
[2] S. De Curtis, S. Moretti, R. Nagai and K. Yagyu, JHEP **10** (2021), 040 [arXiv:2107.08201 [hep-ph]].
[3] S. De Curtis, L. Delle Rose, S. Moretti and K. Yagyu, PoS **EPS-HEP2019** (2020), 344 [arXiv:1910.13699 [hep-ph]].
[4] S. De Curtis, L. Delle Rose, S. Moretti and K. Yagyu, JHEP **12** (2018), 051 [arXiv:1810.06465 [hep-ph]].
[5] S. De Curtis, L. Delle Rose, S. Moretti and K. Yagyu, Phys. Lett. B **786** (2018), 189-194 [arXiv:1803.01865 [hep-ph]].
[6] D. B. Kaplan, Nucl. Phys. B **365** (1991), 259-278
[7] S. De Curtis, S. Moretti, K. Yagyu and E. Yildirim, Eur. Phys. J. C **77** (2017) no.8, 513 [arXiv:1610.02687 [hep-ph]].
[8] S. De Curtis, S. Moretti, K. Yagyu and E. Yildirim, Phys. Rev. D **94** (2016) no.5, 055017 [arXiv:1602.06437 [hep-ph]].
[9] S. De Curtis, S. Moretti, K. Yagyu and E. Yildirim, PoS **CHARGED2016** (2016), 018 [arXiv:1612.05125 [hep-ph]].

[10] G. C. Branco, P. M. Ferreira, L. Lavoura, M. N. Rebelo, M. Sher and J. P. Silva, Phys. Rept. **516** (2012), 1-102 [arXiv:1106.0034 [hep-ph]].
[11] F. Gianotti, M. L. Mangano, T. Virdee, S. Abdullin, G. Azuelos, A. Ball, D. Barberis, A. Belyaev, P. Bloch and M. Bosman, *et al.* Eur. Phys. J. C **39** (2005), 293-333 [arXiv:hep-ph/0204087 [hep-ph]].
[12] S. De Curtis, S. Moretti, K. Yagyu and E. Yildirim, Phys. Rev. D **95** (2017) no.9, 095026 [arXiv:1702.07260 [hep-ph]].
[13] P. Bechtle, O. Brein, S. Heinemeyer, O. Stål, T. Stefaniak, G. Weiglein and K. E. Williams, Eur. Phys. J. C **74** (2014) no.3, 2693 [arXiv:1311.0055 [hep-ph]].
[14] P. Bechtle, S. Heinemeyer, O. Stål, T. Stefaniak and G. Weiglein, Eur. Phys. J. C **74** (2014) no.2, 2711 [arXiv:1305.1933 [hep-ph]].
[15] H. Bahl, T. Biekötter, S. Heinemeyer, C. Li, S. Paasch, G. Weiglein and J. Wittbrodt, Comput. Phys. Commun. **291** (2023), 108803 [arXiv:2210.09332 [hep-ph]].
[16] A. David *et al.* [LHC Higgs Cross Section Working Group], [arXiv:1209.0040 [hep-ph]].
[17] CMS Collaboration, [arXiv:1307.7135 [hep-ex]].
[18] A. Pich and P. Tuzon, Phys. Rev. D **80** (2009), 091702 [arXiv:0908.1554 [hep-ph]].
[19] S. Heinemeyer, W. Hollik and G. Weiglein, Comput. Phys. Commun. **124** (2000) 76.
[20] T. Hahn, S. Heinemeyer, W. Hollik, H. Rzehak and G. Weiglein, Phys. Rev. Lett. **112** (2014) 141801.
[21] E. Bagnaschi *et al.*, LHCHXSWG-2015-002.
[22] G. Panico, M. Redi, A. Tesi and A. Wulzer, JHEP **1303** (2013) 051.
[23] S. Davidson and H. E. Haber, Phys. Rev. D **72** (2005) 035004 [Erratum: Phys. Rev. D **72** (2005) 099902].
[24] H. E. Haber and D. O'Neil, Phys. Rev. D **74** (2006) 015018 [Erratum: Phys. Rev. D **74** (2006) 059905].
[25] H. E. Haber and D. O'Neil, Phys. Rev. D **83** (2011) 055017.
[26] G. Aad *et al.* [ATLAS and CMS Collaborations], JHEP **1608** (2016) 045.
[27] S. De Curtis, L. Delle Rose, F. Egle, M. Mühlleitner, S. Moretti and K. Sakurai, [arXiv:2310.10471 [hep-ph]].
[28] G. Aad *et al.* [ATLAS], Phys. Lett. B **843** (2023), 137745 [arXiv:2211.01216 [hep-ex]].
[29] M. Aaboud *et al.* ATLAS Collaboration, Eur. Phys. J. C **78** (2018) no.7, 565 [arXiv:1804.10823 [hep-ex]].
[30] CMS Collaboration, CMS-PAS-HIG-17-008.
[31] X. Cid Vidal, M. D'Onofrio, P. J. Fox, R. Torre, K. A. Ulmer, A. Aboubrahim, A. Albert, J. Alimena, B. C. Allanach and C. Alpigiani, *et al.* CERN Yellow Rep. Monogr. **7** (2019), 585-865 [arXiv:1812.07831 [hep-ph]].
[32] S. Moretti and D. A. Ross, Phys. Lett. B **712** (2012), 245-249 [arXiv:1203.3746 [hep-ph]].